Acta Pharmacologica Sinica (2017) 38: 806–822
www.nature.com/aps

*Open*

Original Article

# Two birds, one stone: dual targeting of the cancer cell surface and subcellular mitochondria by the galectin-3-binding peptide G3-C12

Wei SUN[1, 2, #], Lian LI[1, #], Li-jia LI[1], Qing-qing YANG[1], Zhi-rong ZHANG[1], Yuan HUANG[1, *]

[1]*Key Laboratory of Drug Targeting and Drug Delivery System, Ministry of Education, West China School of Pharmacy, Sichuan University, Chengdu 610041, China;* [2]*Therapeutic Proteins Key Laboratory of Sichuan Province, Kang Hong Pharmaceutical Group, Chengdu 610036, China*

**Abstract**

Active tumor-targeting approaches using specific ligands have drawn considerable attention over the years. However, a single ligand often fails to simultaneously target the cancer cell surface and subcellular organelles, which limits the maximum therapeutic efficacy of delivered drugs. We describe a polymeric delivery system modified with the G3-C12 peptide for sequential dual targeting. In this study, galectin-3-targeted G3-C12 peptide was conjugated onto the N-(2-hydroxypropyl) methacrylamide (HPMA) copolymer for the delivery of $_D$(KLAKLAK)$_2$ (KLA) peptide. G3-C12-HPMA-KLA exhibited increased receptor-mediated internalization into galectin-3-overexpressing PC-3 cells. Furthermore, G3-C12 peptide also directed HPMA-KLA conjugates to mitochondria. This occurred because the apoptosis signal triggered the accumulation of galectin-3 in mitochondria, and the G3-C12 peptide that specifically bound to galectin-3 was trafficked along with its receptor intracellularly. As a result, G3-C12-HPMA-KLA disrupted the mitochondrial membrane, increased the generation of reactive oxygen species (ROS) and induced cytochrome *c* release, which ultimately resulted in enhanced cytotoxicity. An *in vivo* study revealed that the G3-C12 peptide significantly enhanced the tumor accumulation of the KLA conjugate. In addition, G3-C12-HPMA-KLA exhibited the best therapeutic efficacy and greatly improved the animal survival rate. Our work demonstrates that G3-C12 is a promising ligand with dual-targeting functionality.

**Keywords:** HPMA copolymer; mitochondrial targeting; cancer therapy; KLA peptide; dual targeting

*Acta Pharmacologica Sinica* (2017) 38: 806–822; doi: 10.1038/aps.2016.137; published online 9 Jan 2017

## Introduction

One of the most challenging and clinically important goals in cancer nanomedicine is to deliver therapeutic agents to their target site within a solid tumor[1]. One approach is to add targeting ligands to the nanoparticle surface that can specifically bind to receptors on the cancer cell membrane and undergo increased internalization through receptor-mediated endocytosis[2, 3]. However, nanoparticle accumulation in cancer cells does not necessarily lead to an efficient therapeutic outcome. Nanomedicines seem to lose their targeting capacity intracellularly before mediating their effect in a specific target subcellular organelle (*eg*, the nucleus or mitochondria)[4, 5]. For instance, many RGD-targeted systems are reported to enhance tumor cell uptake via recognition of RGD by integrin $\alpha_v\beta_3$, yet RGD subsequently remained sequestered in the lysosome[6, 7].

In this regard, ligands that are active subcellularly are being developed. The nuclear localization signal (NLS) has been reported to have high affinity for nuclear pore complexes and is thus capable of overcoming the barrier posed by double-layered nuclear envelopes[8]. The lipophilic triphenylphosphonium (TPP) cation is a classic mitochondrial anchor that has been demonstrated to effectively deliver payloads into mitochondria via electrostatic interactions[9]. However, most drugs from solely NLS- or TPP-modified platforms were found to be localized mainly in the plasma membrane, with limited accumulation in the nucleus or mitochondria[10–12]. This indicates that NLS- and TPP-containing drugs with poor cellular penetration and internalization efficiencies cannot exhibit their nucleus- and mitochondria-targeting ability.

These previous experiences suggest that a single ligand with one target site might only achieve suboptimal therapeutic effects, as it cannot overcome both cellular and subcellular barriers at the same time. However, there is a chance that a dual-

[#] These authors contributed equally to this work.
[*] To whom correspondence should be addressed.
E-mail huangyuan0@163.com
Received 2016-07-09 Accepted 2016-09-13

ligand approach could show promise for synergistic cancer therapy. Subcellular-targeting ligands are mostly positively charged and exhibit no selectivity for specific organs, tissues or cell types. Coating the nanoparticle surface with both a subcellular-targeting ligand and a tumor cell-targeting ligand might reduce the targeting efficiency of the latter, thereby even decreasing the accumulation of the drug in tumors[13], which explains why few studies have reported the *in vivo* application of the dual-ligand modification strategy[9]. Moreover, the modification process is complicated by the potential effects of ligand density on targeting efficiency, and so careful screening is needed to determine the density of each ligand that will maximize targeting efficiency[14, 15].

To this end, it is highly desirable to discover a 'magical bullet' with sequential dual-targeting directions. Previously, we identified the G3-C12 peptide, which contains the amino acid sequence ANTPCGPYTHDCPVKR, as a rationally designed galectin-3-targeting ligand that remarkably improves the therapeutic efficacy of an anticancer drug based on N-(2-hydroxypropyl) methacrylamide (HPMA) copolymers both *in vitro* and *in vivo*[3, 16, 17]. In this study, we further demonstrate that the G3-C12 peptide can achieve dual targeting of the cancer cell surface and subcellular mitochondria. In this drug-delivery system, the antibiotic peptide $_D$(KLAKLAK)$_2$ (KLA) was selected as a model drug, because the KLA peptide specifically disrupts the mitochondrial membrane and initiates apoptotic cell death. However, native KLA peptide was reported to have rather poor cell-uptake efficiency, and it often fails to localize in mitochondria[18–21]. Adar *et al* conjugated KLA peptide onto Asn-Gly-Arg (NGR)-targeted HPMA copolymers, and the results showed that NGR could enhance the cellular uptake of KLA-loaded HPMA copolymers, but the mitochondrial accumulation of the copolymers needed to be enhanced[22]. Chu *et al* developed GKRK peptide-modified HPMA-KLA copolymers for mitochondrial targeting. Although the mitochondrial accumulation of HPMA-KLA copolymers was improved to some degree, further enhancement might be restricted due to limited internalization of the GKRK peptide[23]. To achieve effective mitochondrial targeting, we conjugated both the G3-C12 ligand and the KLA peptide onto HPMA copolymers. Our results showed that G3-C12-HPMA-KLA exhibited both enhanced cell endocytosis and subsequent mitochondrial targeting in galectin-3-overexpressing PC-3 cells. The potential mechanism of the G3-C12 peptide-mediated intracellular re-distribution of galectin-3 was studied in detail. G3-C12-HPMA-KLA with sequential dual-targeting ability was also demonstrated to show great promise both *in vitro* and *in vivo* (Scheme 1).

## Materials and methods

### Reagents

The azide-modified KLA peptide ($_D$(KLAKLAK)$_2$-N3) was synthesized using standard solid-phase peptide synthesis by Chinese Peptide Co, Ltd (Hangzhou, China). Cyanine 5.5 NHS ester (Cy5.5-NHS) were purchased from Lumiprobe (Hallandale Beach, FL, USA). 3-(4,5-Dimethyl-2-tetrazolyl)-2, 5-diphenyl-2H tetrazolium bromide (MTT), 4′,6′-diamidino-2-phenylindole (DAPI), Azobisisobutyronitrile (AIBN) and citrus pectin (CP) were purchased from Sigma Chemical Co (St Louis, MO, USA). The galectin-3-binding peptide (G3-C12) was synthesized by KaiJie Biopharm Co, Ltd (Chengdu, China). The scrambled peptide (s)-G3-C12 (sequence: PTHVTCKYCPAGNRPD) was synthesized by GL Biochem Co, Ltd (Shanghai, China). The bicinchoninic acid (BCA) kit and annexin V-fluorescein-5-isothiocyanate (FITC)/propidium iodide (PI) apoptosis detection kit were purchased from KeyGEN, Inc (Nanjing, China). Mito-Tracker Red was purchased from Invitrogen (Carlsbad, CA, USA). Endoplasmic reticulum (ER)-Tracker Red, Golgi-Tracker Red, ROS detection kit and the JC-1 molecular probe were all acquired from Beyotime Institute of Biotechnology (Haimen, China). The mouse anti-cytochrome *c*, rabbit anti-COX IV, rabbit anti-eLGALS3 primary antibodies and FITC-conjugated goat anti-rabbit secondary antibodies were purchased from ABclonal Biotech Co, Ltd (Cambridge, MA, USA). Horseradish peroxidase (HRP)-conjugated goat anti-rabbit secondary antibodies were purchased from ZSGB-BIO (Beijing, China). All other chemicals and reagents were of analytical grade.

### Synthesis of co-monomers

N-(2-hydroxypropyl) methacrylamide (HPMA)[24], N-methacryloyl-glycylglycyl-p-nitrophenyl ester (MA-GG-ONp)[25], N-methacryloyl-aminopropyl-FITC (MA-AP-FITC)[26] and N-methacryloyl-glycylglycyl-propargyl (MA-GG-C≡CH) monomers were synthesized using a modified method that has been reported previously[27].

### Synthesis of G3-C12-HPMA-KLA copolymer

To attach the G3-C13 peptide to HPMA copolymer, we followed our previously established procedures[3]. Briefly, HPMA copolymer precursor with side chains containing *p*-nitrophenyl (ONp) groups and alkynyl groups was prepared by random radical precipitation copolymerization. The reaction was carried out in acetone (using 2,2-azobisisobutyronitrile (AIBN) as an initiator, 2% wt; monomer concentration, 12.5% wt; molar ratio of HPMA monomers:MA-GG-ONp:MA-GG-C≡CH monomers, 80:10:10) under nitrogen in sealed ampoules for 24 h at 50 °C. After evaporating the solvent, the residue was subsequently dissolved in methanol and precipitated with diethyl ether. After drying, the HPMA copolymer precursor appeared as a slightly yellow solid. Then, G3-C12 peptide was conjugated onto the HPMA copolymer precursor upon reaction with reactive ONp groups. Briefly, the above-described HPMA copolymer precursor and G3-C12 peptide were dissolved intodimethyl formamide (DMF) at an equal molar ratio of ONp groups and G3-C12. The reaction mixture was stirred at room temperature for 20 h, followed by dialysis against distilled water for 48 h and freeze drying to yield the G3-C12 peptide-modified HPMA copolymer precursor (G3-C12-HPMA-GG-C≡CH). Scramble (s)-G3-C12 peptide was attached to HPMA copolymer precursor in the same manner.

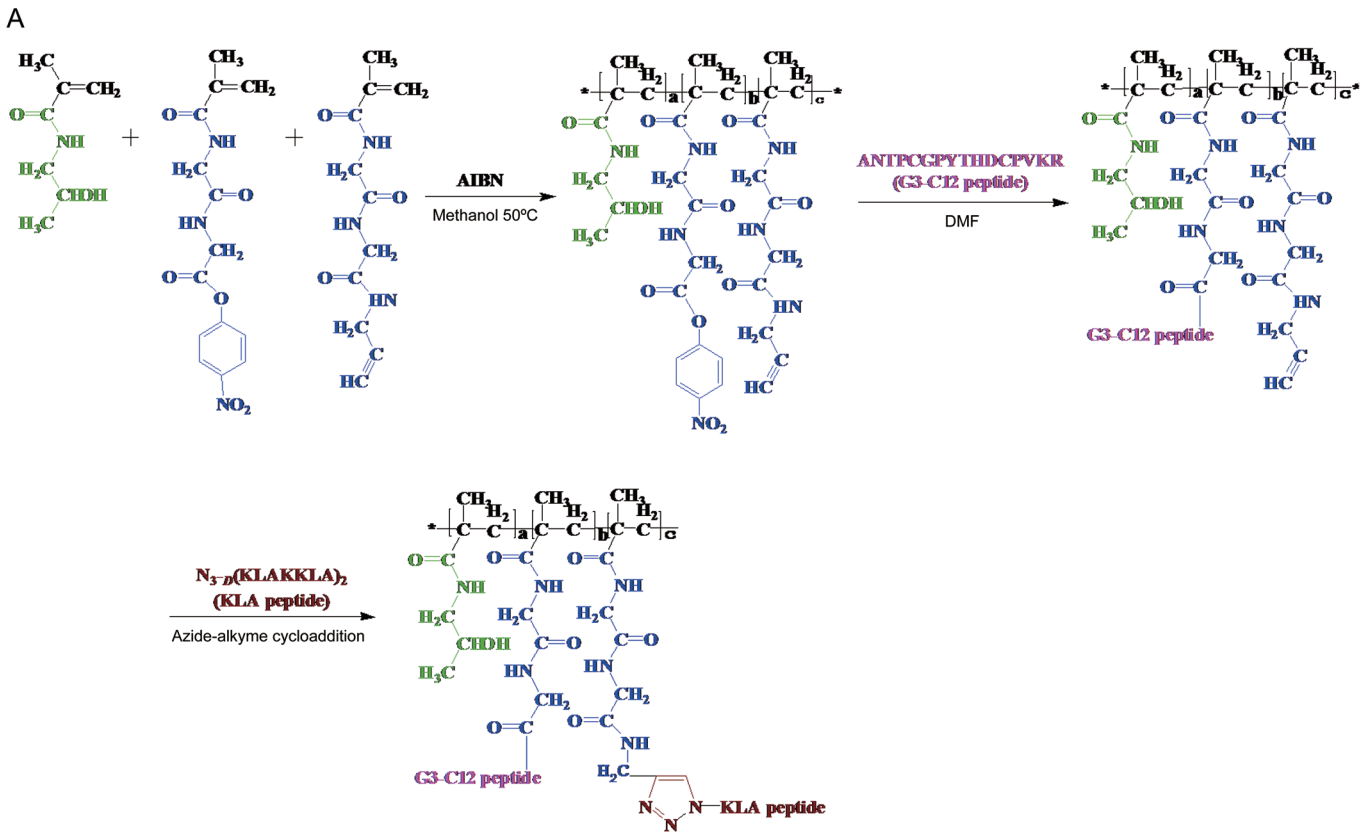


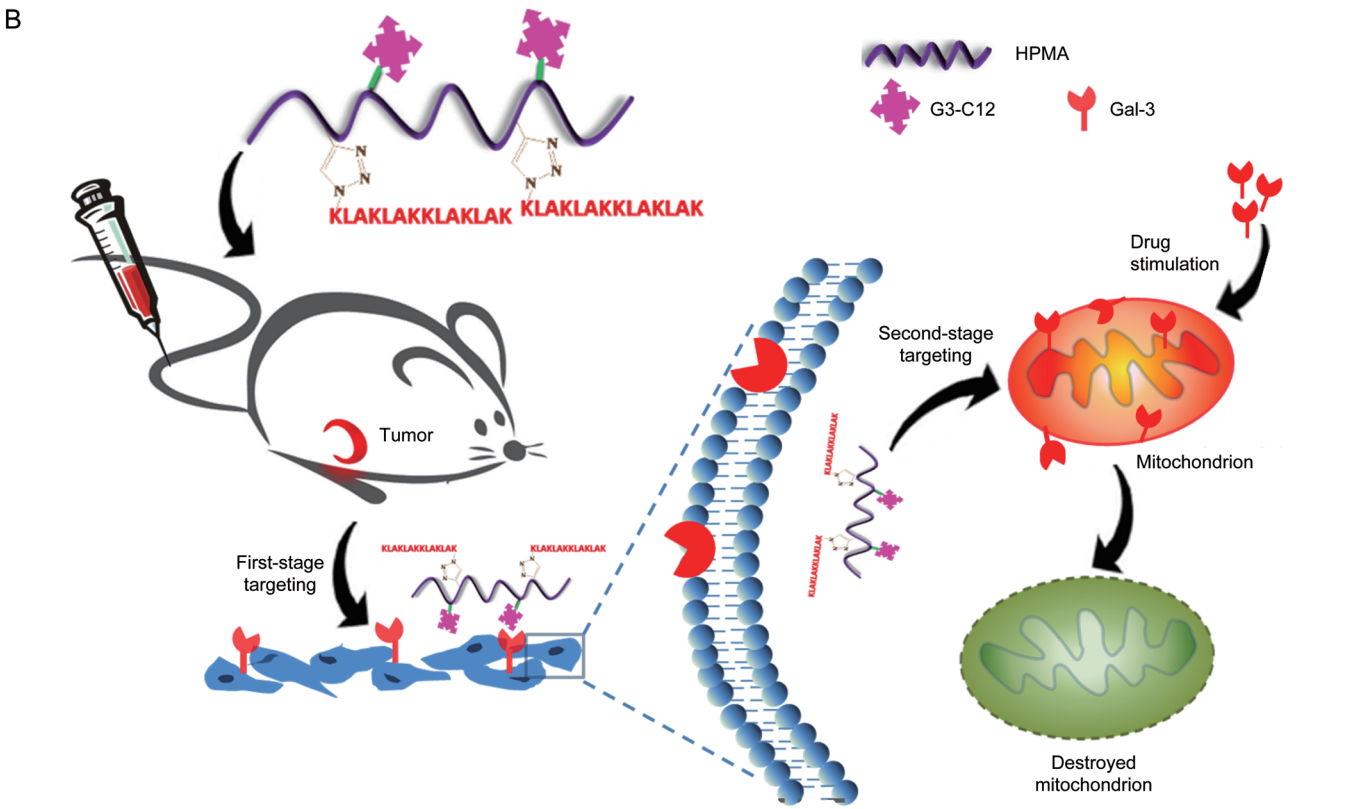


**Scheme 1.** (A) Synthesis route of G3-C12-HPMA-KLA conjugates. (B) Illustration of G3-C12-HPMA-KLA conjugates with sequential dual-targeting functionality from tumor cell surface to intracellular mitochondria.

For conjugation of KLA peptide, azide-modified KLA peptide was conjugated to G3-C12-HPMA-GG-C≡CH using copper-catalyzed azide-alkyne cycloaddition[27]. Briefly, azide-modified KLA peptide, $CuSO_4 \cdot 5H_2O$ and G3-C12-HPMA-GG-C≡CH were dissolved in water/tert-butyl alcohol (1:1, *v*/*v*) with a 1:1 molar ratio of KLA peptide and alkynyl groups. Sodium ascorbate dissolved in water/tert-butyl alcohol (1:1, *v*/*v*) was added to the reaction, which was then stirred for 24 h at room temperature. A large excess of ethylene diaminetetraacetic acid (EDTA) disodium salt (at a concentration >10 times greater than that of Cu by molar ratio) was added to the solution, which was stirred for another 1 h at room temperature and then dialyzed against distilled water to remove unreacted substances. The purity of the solution was assessed using size-exclusion chromatography on a Superose 200 10/300 GL analytical column (Amersham Biosciences, NJ, USA) attached to an AKTA Fast Protein Liquid Chromatography system (Amersham Biosciences). The purified polymer solution was lyophilized to obtain the final G3-C12-HPMA-KLA product.

Fluorophore (FITC/Cy5.5)-labeled HPMA copolymer conjugates were synthesized using similar methods, except that the MA-FITC monomer and MA-Cy5.5 monomer replaced 2 mol% of the HPMA monomer in the random radical copolymerization.

### Characterization of polymers

The molecular weight and polydispersity index (PDI) of the conjugates were estimated using size-exclusion chromatography on a Superose 200 10/300 GL analytical column (Amersham Biosciences, NJ, USA) calibrated with poly(HPMA) fractions using a Fast Protein Liquid Chromatography (AKTA FPLC) system (Amersham Biosciences). The FITC content in the polymers was determined with ultraviolet-visible (UV-vis) spectrometry using $\varepsilon 494 = 80\,000\ L \cdot mol^{-1} \cdot cm^{-1}$ (0.1 mol/L borate buffer, pH 9.0). The conjugation ratio of Cy5.5 to polymer was determined by measuring the fluorescence intensity ($\lambda_{ex}$=676 nm, $\lambda_{em}$=707 nm) in dimethylsulfoxide (DMSO). The G3-C12 or KLA peptide content of the conjugates was determined by analyzing the amino acid content (Commonwealth Biotech Inc, VA, USA). The size distribution and zeta potential of all HPMA copolymers in deionized water (1 mg/mL copolymers) were measured on a Malvern Zetasize NanoZS90 instrument (Malvern Instruments Ltd, Malvern, UK).

### Expression of galectin-3

The expression of galectin-3 in PC-3 and LNCaP cells was measured using Western blot analysis. Approximately $5\times10^6$ cells were harvested, washed with cold phosphate buffer saline (PBS), and lyzed in ice-cold lysis buffer containing protease inhibitors. The lysate was centrifuged at 14 000 rounds per minute for 15 min at 4 °C to collect the supernatant proteins. Equal amounts (30 μg) of total protein were separated by 12% SDS-PAGE and transferred to polyvinylidene difluoride membranes. After incubating with primary antibody against eLGALS3, the membranes were incubated with HRP-labeled goat anti-rabbit secondary antibodies and visualized using Immobilon Western HRP Substrate on a Bio-Rad Chemi-Doc MP System (Bio-Rad Laboratories, USA).

### Quantification of cell uptake by flow cytometry

PC-3 and LNCaP prostate cancer cells were seeded on 12-well plates at a density of $1\times10^5$ cells/well. After incubation for 24 h, the cells were treated with various FITC-labeled HPMA polymer conjugates (0.5 mg/mL copolymers) in the presence and absence of 10 μmol/L free peptide at 37 °C for 4 h. Then, the cells were harvested and analyzed immediately using flow cytometry (Cytomics FC 500, Beckman Coulter, Miami, FL, USA) after washing twice with PBS. The mean fluorescence intensity of $1\times10^4$ cells was recorded for each sample.

### Fluorescence confocal imaging of internalization

PC-3 and LNCaP cells were seeded at $1.5\times10^6$ cells in a 6-cm petri dish for 24 h. The cells were then treated with different polymer conjugates with FITC-labeled subunits (0.5 mg/mL polymers) for 4 h. After treatment, cells were washed with PBS three times. 4′,6-diamidino-2-phenylindole (DAPI) (5 mg/mL) was added to visualize the nuclei 3 min before imaging. Cell fluorescence imaging was performed using a laser-scanning confocal microscope (FV1000, Olympus, Japan).

### Preparation of modified CP (MCP)

pH and temperature modification of CP were performed as previously described[28]. Briefly, CP was solubilized as a 1.5% solution in distilled water, and its pH was increased to 10.0 with NaOH for 1 h at 50–60 °C. The solution was then cooled to room temperature while its pH was adjusted to 3.0 with HCl, and the solution was stored overnight. Samples were precipitated the next day with 95% ethanol and incubated at -20 °C for 2 h, filtered, washed with acetone, and dried on Whatman filters.

### Investigation of colocalization with the mitochondria

Confocal microscopy was used to observe the colocalization of various FITC-labeled HPMA copolymers in the mitochondria. Briefly, PC-3 cells were seeded in chambered coverslips at a density of $1\times10^4$ cells/well. After incubation for 24 h, the cells were treated with G3-C12-HPMA, HPMA-KLA, (s)-G3-C12-HPMA-KLA, G3-C12-HPMA-KLA and MCP plus G3-C12-HPMA-KLA (0.5 mg/mL copolymers), and incubated for an additional 4 h. Then, cells were washed twice with ice-cold PBS and counterstained with 200 nmol/L Mito-Tracker red/blue to label mitochondria or with DAPI to label nuclei according to the manufacturer's instructions. The stained cells were imaged using a laser-scanning confocal microscope with identical settings for each confocal study. Composite images were created by overlapping the images obtained from individual channels.

### Intracellular trafficking of galectin-3 under KLA stimulation

To study the intracellular trafficking of galectin-3 under KLA stimulation, confocal microscopy was used to observe the colo-

calization of galectin-3 and organelles. Briefly, PC-3 cells were seeded at $1\times10^4$ cells/well in chambered coverslips. Then, the cells were treated with 100 μmol/L KLA peptides for an additional 4 h. The cells were then washed with PBS (pH 7.4) and stained with Mito-Tracker probe (200 nmol/L), endoplasmic reticulum (ER)-Tracker probe (500 nmol/L) and Golgi-Tracker probe (150 μg/mL) for 30 min. The cells then were washed twice with PBS, fixed with 4% paraformaldehyde for 15 min, permeabilized using 0.1% Triton X-100 for 5 min, and blocked with 1% bovine serum albumin in PBS for 30 min. After blocking, rabbit anti-eLGALS3 polyclonal antibody was added at a 1:50 dilution, and cells were incubated overnight. Secondary antibody (FITC-labeled goat anti-rabbit IgG; ABclonal) was added at a 1:200 dilution, and cells were incubated for 1 h. The stained cells were imaged using a laser-scanning confocal microscope (FV1000, Olympus, Japan) with identical settings for each confocal study.

### Drug accumulation in isolated mitochondrial fractions

Drug accumulation in the mitochondrial fractions was quantified by flow cytometry[5, 29]. PC-3 cells were seeded in 6-well plates ($4\times10^5$ cells per well) for 24 h, and then G3-C12-HPMA, HPMA-KLA, (s)-G3-C12-HPMA-KLA and G3-C12-HPMA-KLA (0.5 mg/mL copolymers) pretreated with 0.03% MCP were added for 4 h of co-culture. Control experiments were performed by adding only culture medium. The collected cell pellets were washed twice with cold PBS, and mitochondrial isolation was carried out using a cell mitochondria isolation kit (Beyotime Institute of Biotechnology, China). Briefly, cells were resuspended in mitochondrial isolation buffer (provided in the kit) and homogenized with 15 strokes of a homogenizer. The obtained suspensions were centrifuged at $600\times g$ for 10 min, and the supernatant was collected and centrifuged at $11\,000\times g$ for 10 min to pellet the mitochondria. The precipitated mitochondria were collected and resuspended in 0.3 mL PBS buffer (pH 7.4). Copolymer uptake by mitochondria ($1\times10^4$) was measured by flow cytometry, using the fluorescence intensity of loaded FITC. Each assay was repeated in triplicate.

### Cytotoxicity assay

Cytotoxicity was assessed using a tetrazolium dye (MTT) assay based on the reduction of MTT formazan crystals by living cells. PC-3 cells were seeded into 96-well plates at a density of $1\times10^4$ cells/well and cultured for 24 h. For biocompatibility investigation, the cells were treated with drug-free carrier HPMA copolymer (pHPMA) and G3-C12-HPMA copolymer (25–800 mg/mL of copolymers) for 24 h at 37 °C. Meanwhile, the cytotoxicity of drug-loaded copolymers was also investigated. PC-3 cells were incubated with free KLA, HPMA-KLA or G3-C12-HPMA-KLA at different concentrations (6.25–100 μmol/L KLA equivalent) for 24 h at 37 °C. Then, MTT was added (5 mg/mL, 20 μL per well), and cells were incubated for another 4 h. After removal of the supernatant, DMSO was added (150 μL per well) to dissolve the formazan crystals, and the absorption at 570 nm was measured using anenzyme-linked immuno sorbent assay (ELISA) plate reader (Thermo, Microplate Reader 550).

### Apoptosis analysis by flow cytometry

For the apoptosis assay, an annexin V-FITC/PI double-staining method was used. PC-3 cells were treated with free KLA, HPMA-KLA or G3-C12-HPMA-KLA (25 nmol/mL KLA equivalent) for 24 h. At the end of the treatment, the cells were trypsinized, washed with PBS and centrifuged at 3000 rounds per minute for 5 min. Then, the cells were resuspended in 500 μL binding buffer and stained with 5 μL annexin V-FITC and 5 μL PI. The cells were incubated in the dark at room temperature for 15 min. Finally, the stained cells were collected for flow cytometric analysis (Cytomics™ FC 500, Beckman Coulter, Miami, FL, USA).

### Mitochondrial depolarization

The mitochondrial membrane potential (MMP; $\Delta\psi m$) was measured using the fluorescent dye JC-1 (Molecular Probes)[30]. After treatment with free KLA, HPMA-KLA or G3-C12-HPMA-KLA (25 nmol/mL KLA equivalent) for 24 h, PC-3 cells were incubated with 5 μg/mL JC-1 for 30 min. The washed cells were then analyzed using flow cytometry, and the ratio of red to green signal was calculated.

### ROS generation

Changes in ROS production were monitored by measuring the oxidative conversion of cell-permeable 2′,7′-dichlorofluorescein diacetate (DCFH-DA) to fluorescent dichlorofluorescein (DCF)[31]. Briefly, PC-3 cells were treated with free KLA, HPMA-KLA or G3-C12-HPMA-KLA (25 nmol/mL KLA equivalent) for 24 h. The cells were then harvested by centrifugation, washed twice with PBS, resuspended in PBS and incubated with 10 μmol/L DCFH-DA for 30 min in the dark. The intracellular ROS levels were then examined immediately by measuring the fluorescence intensity of DCF using flow cytometry.

### Cytochrome *c* release

The expression level of cytochrome *c* in PC-3 cells was measured using Western blot analysis[32]. PC-3 cells were treated with free KLA, HPMA-KLA or G3-C12-HPMA-KLA (25 nmol/mL KLA equivalent) for 24 h. PC-3 cells were then washed twice with ice-cold PBS (pH 7.4) and resuspended in 100 mL of ice-cold mitochondrial buffer 20 mmol/L N-2-hydroxyethylpiperazine-N′-2-ethane-sulfonic acid (HEPES), 1.5 mmol/L $MgCl_2$, 10 mmol/L KCl, 1 mmol/L EDTA, 1 mmol/L ethyleneglycoltetraacetic acid (EGTA), 1 mmol/L dithiothreitol (DTT), and a cocktail of protease inhibitors) containing 250 mmol/L sucrose. The nuclei, mitochondria and unbroken cells were separated from the cytosolic fraction by centrifugation at $10\,000\times g$ for 10 min. The resultant cytosolic fractions from 30 μg protein-equivalent cells were loaded onsodium dodecyl sulfate polyacrylamide gel electrophoresis (SDS-PAGE) gels (12% acrylamide) and evaluated using Western blotting.

### *In vivo* imaging and biodistribution analysis

To trace the distribution of polymer conjugates in the tumor-bearing mice, three mice per group were intravenously administered free Cy5.5, HPMA-KLA-Cy5.5 and G3-C12-HPMA-KLA-Cy5.5, and the near-infrared reflection (NIR) fluorescence images were observed at pre-determined time points (24, 48, and 72 h). To compare the tumor distributions of the above samples, mice were sacrificed 48 h post injection. Tumors were dissected, washed with normal saline and imaged immediately using the *in vivo* imaging system. All the animals used received care in compliance with the guidelines outlined in the Guide for the Care and Use of Laboratory Animals, and all procedures were approved by Sichuan University Animal Care and Use Committee.

### *In vivo* antitumor efficacy

PC-3 tumor-bearing nude mice were randomly divided into five groups ($n$=5 per group) and intravenously injected with saline, free KLA, HPMA-KLA, (s)-G3-C12-HPMA-KLA or G3-C12-HPMA-KLA at a dose of 2.5 nmol/g KLA peptide of mouse body weight in 100 μL saline solution once every other day in the first week and once on the first day in the following weeks. Tumor weights were determined on d 17 post injection. The tumor width and length were measured every 2 d from d 1, and tumor size was calculated using the following formula: (length×width$^2$)/2. Curves showing tumor growth over 3 weeks were generated.

### Histological analysis

For histology, the tumor and main organs were removed from the drug-treated mice on d 21, fixed in 10% paraformaldehyde and embedded in paraffin blocks. The embedded specimens were cut into 4 mm slices, the organs and tumors were stained with hematoxylin and eosin (H&E), and tumors were stained with a caspase-3 antibody and a Ki67 antibody and then visualized with dye-conjugated secondary antibodies under an optical microscope. For transferase-mediated dUTP nick end-labeling (TUNEL) staining, the experiment was conducted by following the instruction manual provided with the *In Situ* Cell Death Detection kit (Roche, Indianapolis, IN, USA).

## Results

### Characterization of HPMA polymers

We first conjugated the G3-C12 ligand to the HPMA copolymer via amidation. Then, KLA peptide was conjugated to the HPMA copolymer via click chemistry. The fabricated G3-C12-HPMA-KLA had a molecular weight of approximately 30 kDa (Figure 1). For various purposes, other copolymers such as non-targeted, FITC-modified and Cy5.5-modified conjugates were also synthesized as controls. The zeta potentials of these copolymer conjugates were only mildly positive, ranging from 1.45 to 3.98 mV. All the copolymer conjugates were of a similar size of (approximately 12 nm). Their characteristics are summarized in Table 1.

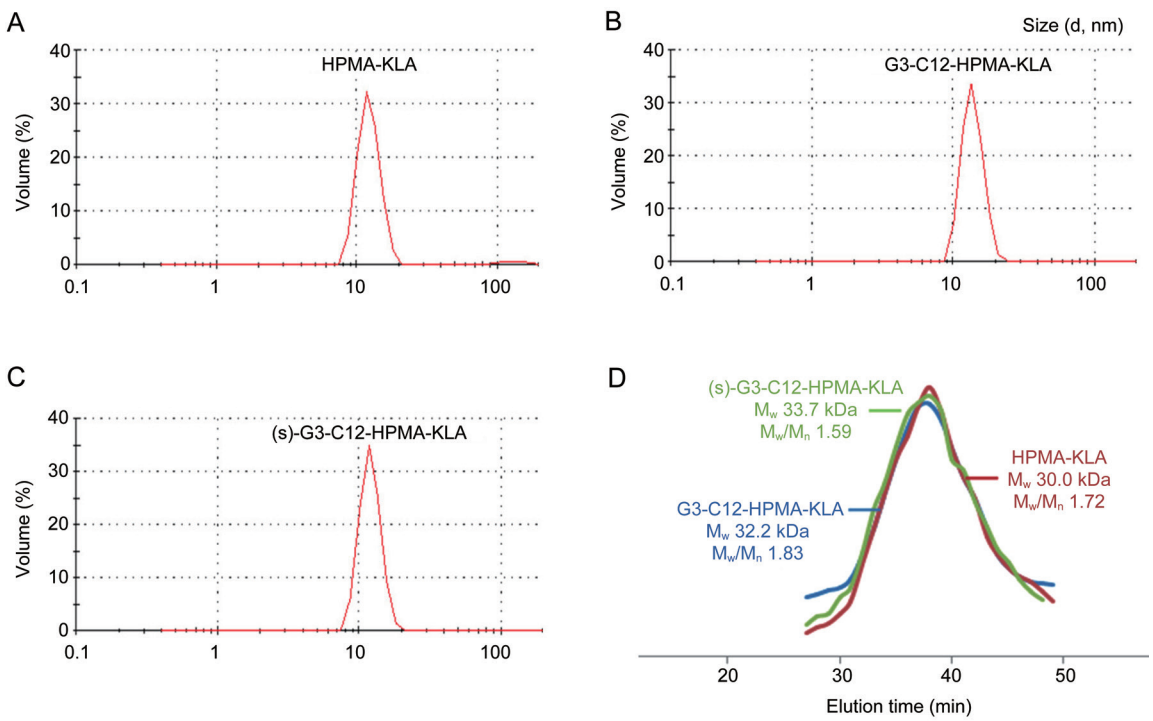


**Figure 1.** Size distribution of (A) HPMA-KLA, (B) G3-C12-HPMA-KLA, (C) (s)-G3-C12-HPMA-KLA copolymers were determined by dynamic light scatter. (D) FPLC chromatograms for HPMA-KLA, G3-C12-HPMA-KLA, (s)-G3-C12-HPMA-KLA copolymers.

**Table 1.** Characteristics of the synthesized HPMA copolymer conjugates containing different functional groups.

| Polymer conjugates | G3-C12 (wt %) | KLA (wt %) | Cy5.5 (wt %) | FITC (wt %) | Mw (kDa) | PDI | Zeta potential (mV) | Size (nm) | PDI |
|---|---|---|---|---|---|---|---|---|---|
| G3-C12-HPMA | 9.74 | | | | 26.6 | 1.52 | 3.98±0.40 | 12.31±0.25 | 0.25 |
| HPMA-KLA | | 19.15 | | | 30.0 | 1.72 | 2.89±0.57 | 12.01±0.35 | 0.26 |
| G3-C12-HPMA-KLA | 9.14 | 18.87 | | | 32.2 | 1.83 | 3.34±0.92 | 12.68±0.14 | 0.25 |
| (s)-G3-C12-HPMA-KLA | 10.32 | 18.93 | | | 33.7 | 1.59 | 2.21±0.23 | 14.21±0.31 | 0.30 |
| G3-C12-HPMA-FITC | 9.38 | | | 5.53 | 30.2 | 1.41 | 1.69±0.34 | 11.20±0.43 | 0.19 |
| HPMA-KLA-FITC | | 18.58 | | 5.99 | 25.4 | 1.26 | 2.95±0.24 | 10.23±0.27 | 0.29 |
| G3-C12-HPMA-KLA-FITC | 10.4 | 17.13 | | 5.52 | 26.2 | 1.20 | 3.21±0.42 | 14.48±0.16 | 0.28 |
| (s)-G3-C12-HPMA-KLA-FITC | 10.73 | 20.12 | | 5.93 | 31.3 | 1.69 | 1.45±0.26 | 15.26±0.31 | 0.25 |
| HPMA-KLA-Cy5.5 | | 19.24 | 2.53 | | 28.8 | 1.57 | 2.51±0.36 | 13.21±0.40 | 0.24 |
| G3-C12-HPMA-KLA-Cy5.5 | 10.9 | 18.24 | 2.49 | | 26.5 | 1.64 | 3.43±0.15 | 13.92±0.37 | 0.31 |

Abbreviations: Mw, weight-averaged molecular weight; PDI, polydispersity index; FITC, fluorescein isothiocyanate; Cy5.5, cyanine 5.5.

### G3-C12 peptide exerts first-stage targeting to the cell surface

We next investigated galectin-3 expression on two prostate cancer cell lines: LNCaP and PC-3. Figure 2A shows that a significantly larger amount of galectin-3 was expressed on PC-3 cells than on the LNCaP cells, which agrees well with previous reports[33]. Because the LNCaP cells express low levels of galectin-3 protein, the amount of G3-C12-HPMA-KLA internalized by the LNCaP cells was similar to the amount of non-targeted HPMA-KLA internalized (Figure 2B). In contrast, cell uptake of G3-C12-HPMA-KLA was significantly higher than that of HPMA-KLA in PC-3 cells, which highly express galectin-3 (Figure 2C). Meanwhile, the scrambled G3-C12-peptide-modified drug conjugate (s)-G3-C12-HPMA-KLA did not show higher cell uptake compared than HPMA-KLA, indicating that the potential targeting effect of the G3-C12 peptide is sequence-dependent. To further confirm the specificity of the G3-C12 peptide, cell internalization of G3-C12-HPMA-KLA in the presence and absence of free G3-C12 peptide were compared. The results showed that free G3-C12 peptide significantly decreased uptake of G3-C12-HPMA-KLA by PC-3 cells (Figure 2C). Moreover, the confocal microscopy images in Figures 2D and 2E confirm that G3-C12-HPMA-KLA was internalized more efficiently into PC-3 cells via specific receptor-mediated endocytosis and further demonstrate that G3-C12 completed the first stage of targeting to the cell surface.

### The G3-C12 peptide exerts second-stage targeting to mitochondria

After active endocytosis, the macromolecular copolymers were directed into lysosomal compartments. Thus, it is highly important to achieve lysosomal escape before mitochondrial localization. Figure 3A shows that during the first 2 h, all the tested copolymers were internalized into the lysosome. As time progressed to 4 h, HPMA-KLA and (s)-G3-C12-HPMA-KLA were still sequestered in the lysosome, while a great proportion of G3-C12-HPMA-KLA had left the lysosome.

Next, we evaluated whether the G3-C12 peptide would exert a second stage of targeting to a subcellular organelle, the mitochondrion. By using the 3D reconstruction of the colocalization experiments, Figure 3B shows the extent to which FITC-labeled KLA-loaded HPMA conjugates colocalized with mitochondria. Z-axis colocalization analysis of confocal micrographs revealed that the scrambled G3-C12 peptide-modified (s)-G3-C12-HPMA-KLA conjugate had limited cell internalization as well as low colocalization with mitochondria. By contrast, significantly more G3-C12-HPMA-KLA conjugates entered the cells, and a much greater proportion of the G3-C12 targeted conjugates localized in mitochondria. This result eliminated the possibility of non-specific interactions between mitochondria and the G3-C12 peptide due to the physicochemical properties of its amino acids and further confirmed that the mitochondrial targeting is indeed mediated by the G3-C12 peptide. Furthermore, quantitation of the accumulation of these conjugates in mitochondria using flow cytometry correlated well with the above results (Figure 3C).

### Both G3-C12 and KLA peptides are indispensable for mitochondrial targeting

To verify the potential mechanisms behind the dual-targeting functionality, we first investigated whether the compositions of the HPMA polymeric system, G3-C12 and KLA peptides were involved. In the absence of G3-C12 peptide (Figure 4A), the HPMA-KLA conjugate did not enter the cell or colocalize with mitochondria as effectively as G3-C12-HPMA-KLA. On the other hand, when lacking the KLA peptide, G3-C12-HPMA exhibited increased cell uptake only and insufficient targeting to mitochondria (Figure 4B). These results were also in line with the quantitative results obtained via flow cytometry (Figure 4C). Thus, both the G3-C12 peptide and the KLA peptide play crucial roles in activating the mitochondrial targeting of the HPMA conjugates.

### KLA triggers the intracellular re-distribution of galectin-3 to mitochondria

As the G3-C12 peptide was previously demonstrated to have high affinity for galectin-3[34] and to be intracellularly traf-

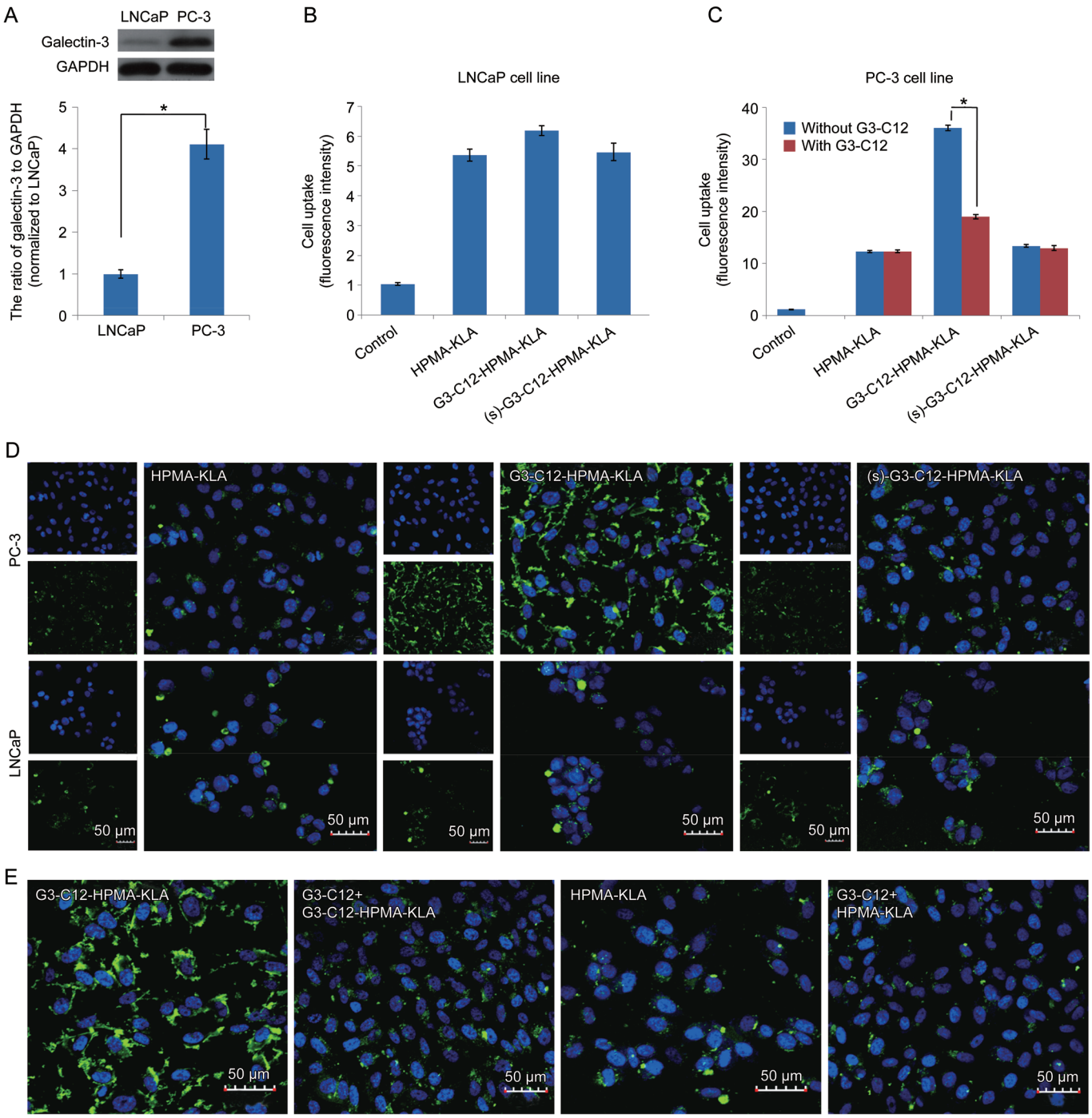


**Figure 2.** (A) Expression of galectin-3 protein in PC-3 cells and LNCaP cells determined by Western Blot. The cell uptake investigation by flow cytometry after 4 h of incubation with LNCaP cells (B) and PC-3 cells (C) in the presence and absence of free peptide. (D) Confocal laser scanning microscopy (CLSM) images of various copolymers treated PC-3 cells and LNCaP cells. The FITC-labeled copolymers and cell nucleus were visualized by green and blue fluorescence, respectively. (E) CLSM imagings of copolymer internalization in the presence and absence of free G3-C12 peptide by PC-3 cells. $^{*}P<0.05$.

ficked along with galectin-3 upon specific binding[16], we suspected that KLA may trigger the re-distribution of galectin-3 to mitochondria. This is a reasonable hypothesis, because in response to a pro-apoptotic stimulus such as a therapeutic agent, the threatened cell would initiate a self-defense mechanism, and galectin-3 could exert its protective effect by gathering in the mitochondria and preventing a decrease in MMP[35, 36]. Thus, we next evaluated the intracellular distribution of galectin-3 in relation to various organelles, which were quantified via scan length-intensity and ImageJ software after KLA stimulation. Figure 5A shows that the galectin-3 distributed randomly in the cytoplasm before KLA stimula-

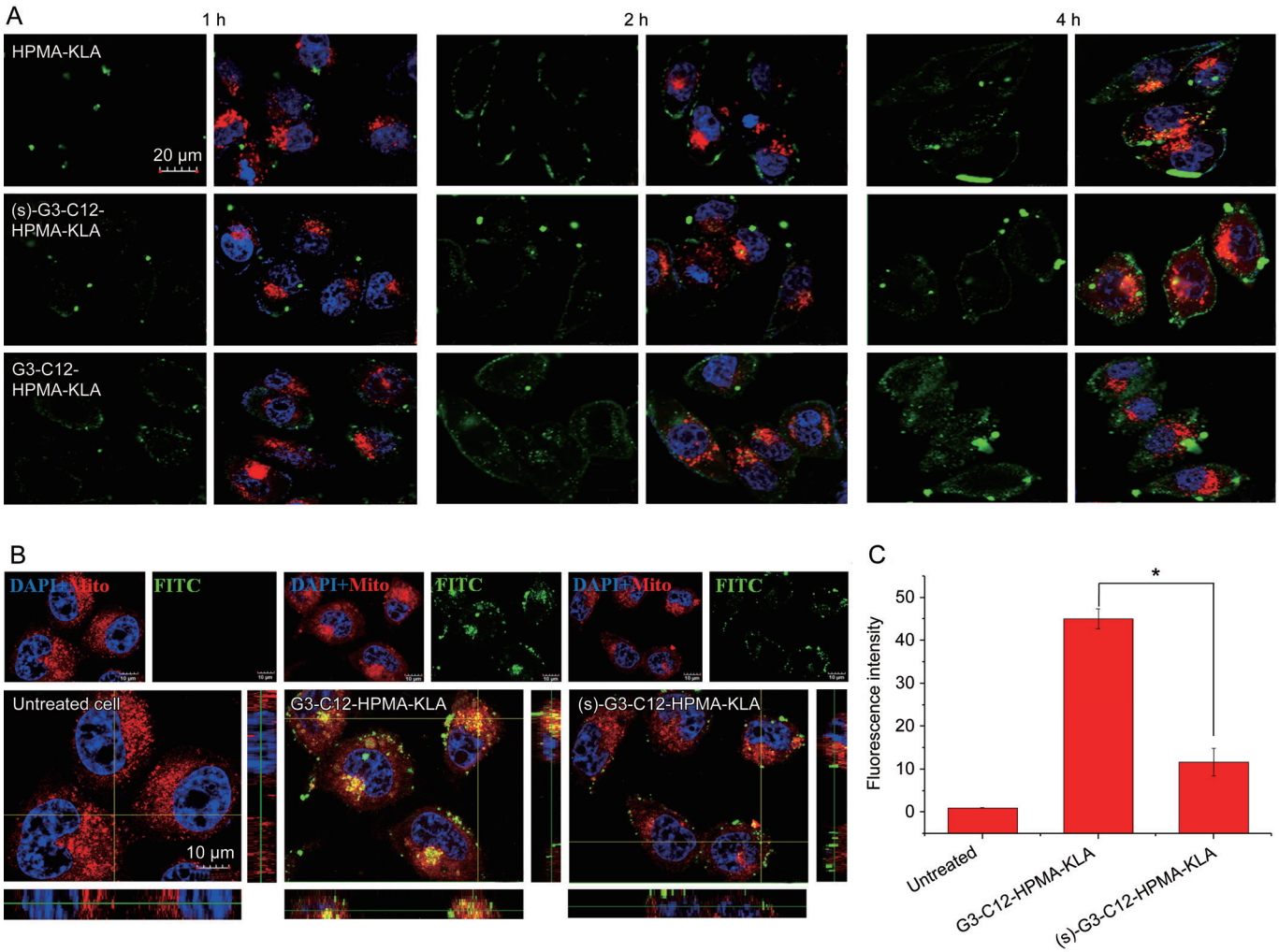


**Figure 3.** (A) Confocal micrographs showing the escape of G3-C12-HPMA-KLA from the lysosome. Yellow color denotes the overlay of FITC fluorescence (green) and lysosome staining (red), while blue shows DAPI staining of nuclei. (B) Z-stack images of subcellular distribution of G3-C12 and scramble G3-C12 peptide modified KLA-loaded HPMA copolymers in PC-3 cells. PC-3 cells were incubated with G3-C12-HPMA-KLA and (s)-G3-C12-HPMA-KLA copolymers for 4 h and then stained with Mito-Tracker Red. Yellow spots in the merged pictures denote the co-localization of the copolymers within mitochondrial compartments. (C) Accumulation of FITC-labeled HPMA copolymers in mitochondria in PC-3 cells measured by flow cytometry. Data are presented as mean±SD ($n$=3). $^{*}P$<0.05.

tion. However, after pretreatment with the KLA peptide, galectin-3 concentrated in the mitochondria with a higher degree of colocalization than was observed without pretreatment (Figure 5B), which agreed well with our hypothesis. By comparison, there was less extensive colocalization of galectin-3 with the ER (Figure 5C) and the Golgi (Figure 5D).

### Mitochondrial targeting relies on the mitochondrial translocation of galectin-3

Next, we inhibited the mitochondrial translocation of galectin-3 using MCP[37]. As shown in Figure 6A, MCP itself did not reduce the total amount of galectin-3 in the cell, nor did it decrease the presence of galectin-3 in mitochondria. As measured by the Western blot in Figure 6B, treatment with the KLA peptide increased the accumulation of galectin-3 in mitochondria, which was in line with the above results. However, when the cells were treated with MCP and KLA together, mitochondrial galectin-3 decreased. Additionally, confocal microscopy showed that galectin-3 did not distribute effectively in mitochondria after MCP+KLA treatment (Figure 6C), which was distinctly different from the non-MCP-treated group (Figure 5B). All these results confirmed that MCP could inhibit the mitochondrial translocation of galectin-3, even after the stimulation of apoptosis with KLA.

Next, we investigated the intracellular distribution of the G3-C12-HPMA-KLA conjugate in the presence of MCP. As shown in Figure 6D and 6E, MCP significantly decreased the colocalization of G3-C12-HPMA-KLA in mitochondria compared with the colocalization observed in the absence of MCP. This could be ascribed to the fact that MCP prevented galectin-3 from being trafficked to mitochondria. Therefore, the G3-C12 peptide, which specifically binds to galectin-3

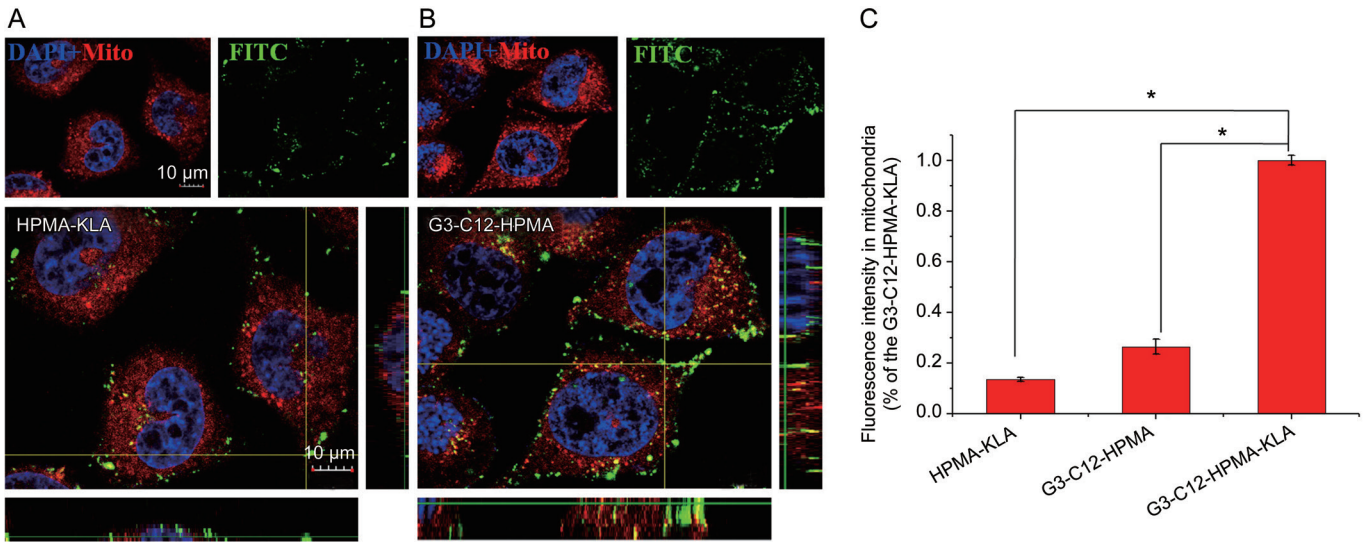


**Figure 4.** Z-stack images of non-ligand modified and drug-free HPMA copolymers subcellular distribution in PC-3 cells. PC-3 cells were incubated with (A) HPMA-KLA and (B) G3-C12-HPMA for 4 h and then stained with Mito-Tracker Red. (C) Quantified analysis of FITC-labeled HPMA copolymers accumulated in mitochondria in PC-3 cells measured by flow cytometry. Data are presented as mean±SD ($n$=3). $^{*}P$<0.05.

and travels along with galectin-3 intracellularly, also lost its mitochondrial-targeting functionality. Here, we found that the sequential dual-targeting mechanisms of G3-C12 strongly depend on its binding to the receptor galectin-3, which is overexpressed on the cell surface and subsequently transported to mitochondria after apoptosis is stimulated.

### The G3-C12 peptide increases cytotoxicity and the pro-apoptotic effect of KLA peptide

The KLA peptide can inhibit cell proliferation by disrupting the mitochondrial membrane[20]. However, its inability to cross the cell membrane and localize in mitochondria, due to multiple intracellular barriers, poses daunting challenges[21, 38]. With the sequential dual-targeting functionality of the G3-C12 peptide of the cell surface and the mitochondria, we expected that G3-C12 could potentiate the cytotoxicity of the KLA peptide. First, we investigated the biocompatibility of the drug-free carrier HPMA copolymer and the G3-C12-HPMA copolymer. The results in Figure 7A show that the drug-free HPMA copolymer and the G3-C12-HPMA copolymer were very biocompatible and did not decrease cell viability even at the highest tested concentration (0.8 mg/mL). Figure 7B shows the cell viabilities after exposure to KLA, HPMA-KLA or G3-C12-HPMA-KLA. The results indicate that G3-C12-HPMA-KLA exhibited greater inhibition of cell proliferation than the free KLA peptide group and the HPMA-KLA group. These findings also correlated with a substantial enhancement of apoptosis induction after treatment with G3-C12-HPMA-KLA compared with KLA peptide alone or non-modified HPMA-KLA (Figure 7C).

### The G3-C12 peptide potentiates apoptosis through the mitochondrial pathway

A decrease in MMP is usually an indicator of mitochondrial dysfunction[39]. Here, we measured the MMP using JC-1 dye as the sensor. JC-1 tends to aggregate (with red fluorescence) in normal mitochondria, and the color changes from red to green when the membrane potential collapses. Therefore, the ratio of red to green fluorescence can be used to assess the status of mitochondria. As shown in the flow cytometry analysis (Figure 8A and 8B), exposure of PC-3 cells to G3-C12-HPMA-KLA resulted in the greatest reduction in MMP when compared with free KLA and HPMA-KLA after 24 h treatment. Figure 8C shows that both HPMA-KLA and G3-C12-HPMA-KLA disrupted the mitochondrial membrane in a time-dependent manner, as revealed by a decrease in red fluorescence and an increase in green fluorescence. However, the G3-C12 peptide clearly accelerated the effect of decreasing the MMP of PC-3 cells. The rapid decrease in MMP also resulted in a morphology change in G3-C12-HPMA-KLA-treated PC-3 cells, especially after 8 h of treatment. The increase in ROS generation and cytochrome *c* release is also a primary indicator of a disrupted mitochondrial membrane[31, 40, 41]. As revealed in Figure 8D and 8E, G3-C12-HPMA-KLA treatment generated the highest ROS levels and triggered the most cytochrome *c* release from mitochondria into the cytosol when compared with HPMA-KLA, KLA or the addition of culture medium alone. These results indicated that the G3-C12-modified vehicle could deliver the KLA peptide to intracellular mitochondria with high efficiency and subsequently exert higher therapeutic efficacy than other vehicles tested by disrupting the mitochondrial membrane.

### The G3-C12 peptide enhances the *in vivo* tumor accumulation and anticancer efficacy of KLA

Before evaluating the therapeutic effect *in vivo*, we investigated whether the G3-C12 targeting peptide could enhance the accumulation of KLA conjugates in tumors in nude mice.

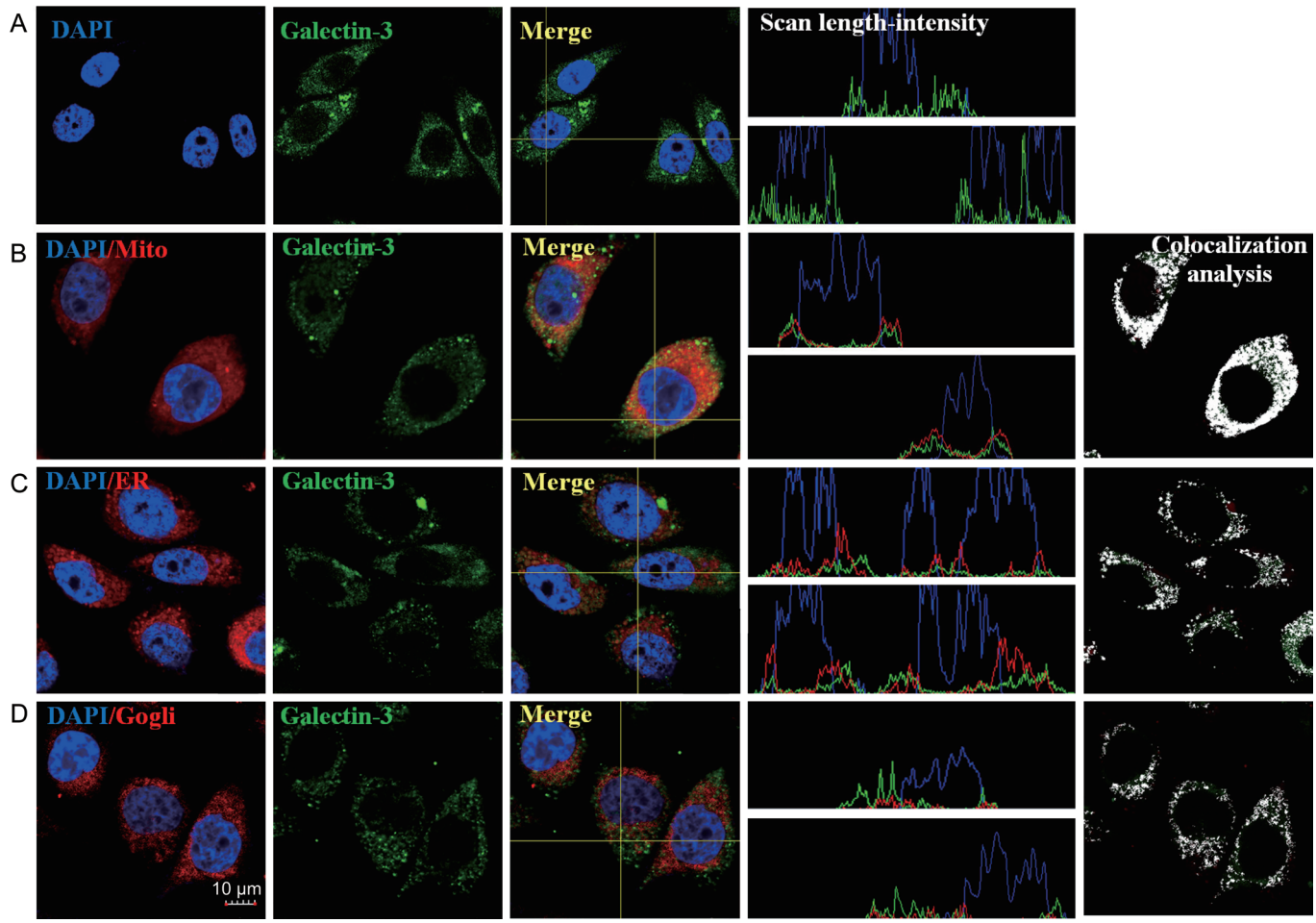


**Figure 5.** Confocal microscopy and line-scan profiles of fluorescence intensity of galectin-3 in PC-3 cells under 4 h stimulation of 100 μmol/L free KLA peptide. PC-3 cells were costained with green staining of (A) blank control, (B) Mito tracker, (C) ER tracker, (D) Gogli tracker, anti-galectin-3 antibody/FITC-conjugated secondray antibody (green staining) and DAPI (blue staining). Yellow spots in pictures denote the co-localization of the galectin-3 within mitochondrial compartments. The blue, green and red curve in the line-scan profiles represents the fluorescence intensity from DAPI, FITC and organelle-tracker Red respectively. White indicates the colocalization of organelle (red) and galectin-3 (green) analyzed using ImageJ software.

As shown in Figure 9A and 9B, both G3-C12-HPMA-KLA and HPMA-KLA displayed a much higher tumor accumulation than the small-molecule free Cy 5.5, which was barely detectable 3 d after intravenous administration, thus highlighting the importance of the enhanced permeability and retention (EPR) effect in *in vivo* application[42, 43]. It is noteworthy that G3-C12-HPMA-KLA also accumulated more favorably in tumors than did non-targeted HPMA-KLA. The G3-C12 peptide might enhance tumor accumulation via the active recognition of galectin-3, which is overexpressed on the PC-3 cancer cell surface.

Mice bearing a subcutaneous PC-3 tumor were intravenously injected with free KLA peptide, HPMA-KLA and G3-C12-HPMA-KLA according to the administration timeline in Figure 9C. Rapid tumor growth was observed in the mice that received saline control. Free KLA peptide treatment resulted in a mild inhibition of tumor growth. By contrast, treatment with HPMA-KLA resulted in greater tumor growth suppression than free KLA, which reflected the enhanced-permeability and retention (EPR) effect of the HPMA copolymer. In addition, G3-C12-HPMA-KLA inhibited the rate of tumor growth to the greatest extent, suggesting that the G3-C12-peptide-modified copolymer could actively deliver KLA to tumors and further localize to the mitochondria where KLA acts, thus improving its therapeutic efficacy *in vivo*. This finding was also consistent with the excised tumor morphology and weights in Figure 9D. Moreover, compared with free KLA peptide and HPMA-KLA, G3-C12-HPMA-KLA significantly improved the survival rate of the animals (Figure 9E).

Cell proliferation and apoptosis in the tumor tissue after treatment was further analyzed by using immunohistochemistry. We performed caspase-3 and Ki67 immunolabeling and a TUNEL assay to assess mitochondria-mediated apoptosis, tumor cell proliferation and apoptosis, respectively (Figure 10A). As expected, the G3-C12-HPMA-KLA treatment, which achieved the highest inhibition of tumor growth rate, induced the most severe mitochondria-mediated apoptosis

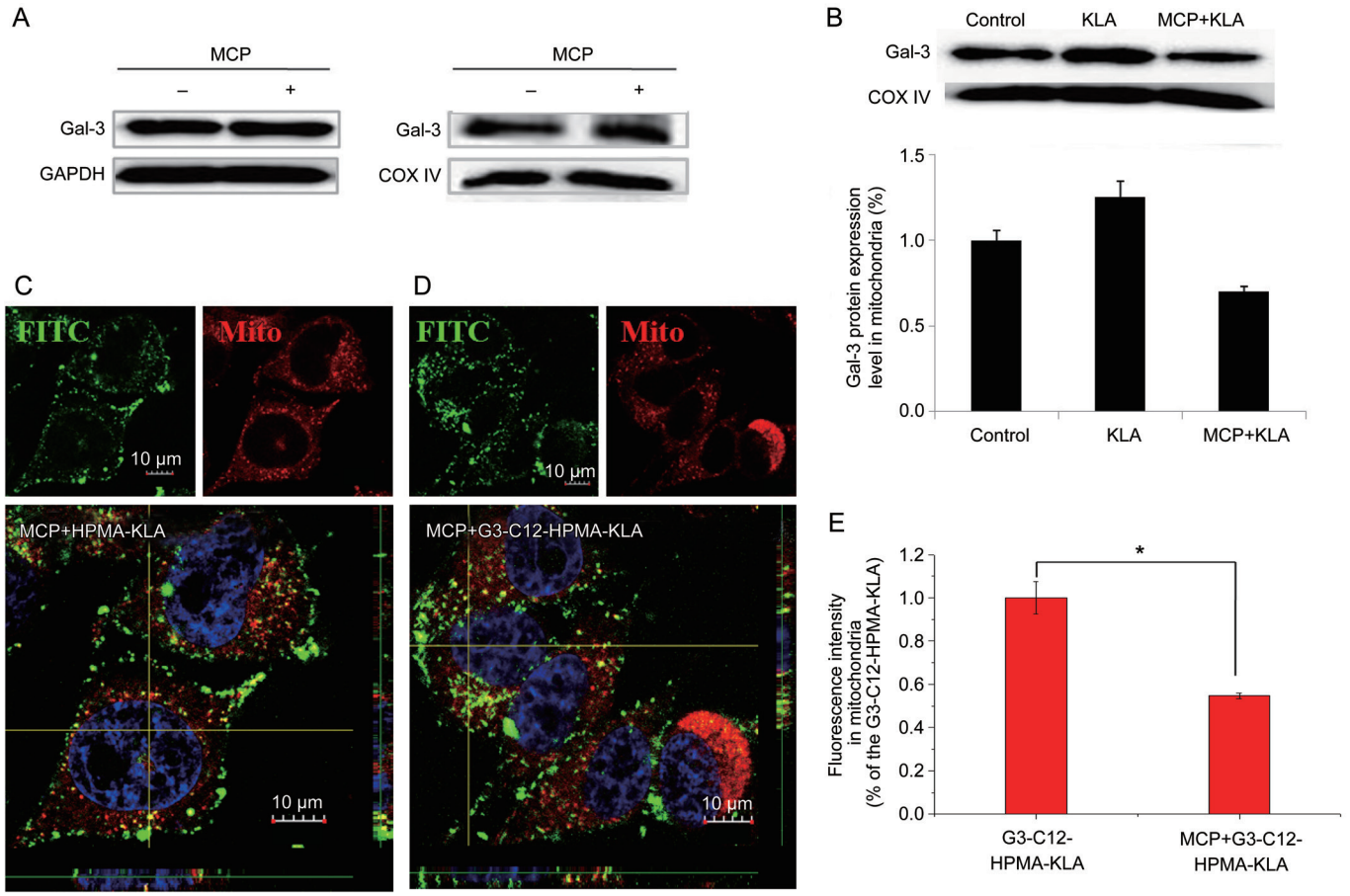


**Figure 6.** (A) Western blot analyzed the galectin-3 expression level after treated inhibitor MCP in PC-3 cells and mitochondria. Samples were run at equal protein concentration and immunostained against cell markers (GAPDH) and mitochondrial marker (COX IV). (B) Western blot analyzed the galectin-3 protein translocated in mitochondria under the stimulation of KLA or KLA puls MCP. (C) Z-stack images of subcellular distribution of galectin-3 after treatment with 100 μmol/L KLA plus MCP. (D) Representative images of mitochondrial distribution of FITC-labeled G3-C12-HPMA-KLA pretreated with inhibitor MCP. (E) Flow cytometry analyzed the accumulation of G3-C12-HPMA-KLA plus MCP in mitochondrial of PC-3 cells. Data are presented as mean±SD ($n$=3). $^{*}P$<0.05.

in tumors. Meanwhile, compared with the administration of free KLA peptide and HPMA-KLA, the administration of G3-C12-HPMA-KLA markedly decreased the number of Ki67-positive proliferating cells and increased the number of TUNEL-positive apoptotic cells in tumors, demonstrating the efficacy of G3-C12-HPMA-KLA in treating PC-3 prostate tumors. The H&E staining in Figure 10B also indicated that G3-C12-HPMA-KLA could increase apoptosis and necrosis in tumors but exhibited no toxicity in other major organs.

## Discussion

Targeted delivery of KLA peptide to mitochondria has long been a great challenge due to the lack of efficient penetration through cell membrane and precise location in mitochondria[20, 44, 45]. Generally, two strategies are frequently used. One is to use ligand that specifically targets the receptor expressed on cell surface or the mitochondria membrane[7, 9]. But seldom ligand could exert dual targeting ability while co-modification of two ligands can sometimes leads to antagonism and complicate the fabrication process[13]. The other strategy is the modification of cationic group that take advantage of electrostatic attraction between the positive charged system and highly negatively charged mitochondria membrane[12, 46]. Unfortunately, this method is regarded as non-specific and can face huge problems when applied *in vivo*[9, 47]. Therefore, it is extremely important to design a system that could target the mitochondria with efficiency and selectivity.

G3-C12 ligand have been demonstrated to exert sequential targeting from cell membrane to intracellular mitochondria. The mechanisms behind this exciting result also differ from those above-mentioned strategies. The active interaction between the G3-C12 ligand and its receptor galectin-3 presents the first stage of targeting to the cancer cell with significantly improved endocytosis. The galectin-3 re-distribution to mitochondria in response to the intracellular signal contributes to the second stage of targeting to subcellular mitochondria. After delivered to its site of action, KLA peptides effectively cause the mitochondria depolarization followed by the cytochrome *c* release, which activates the caspase-3 and leads to apoptosis. This platform has also been demonstrated to be

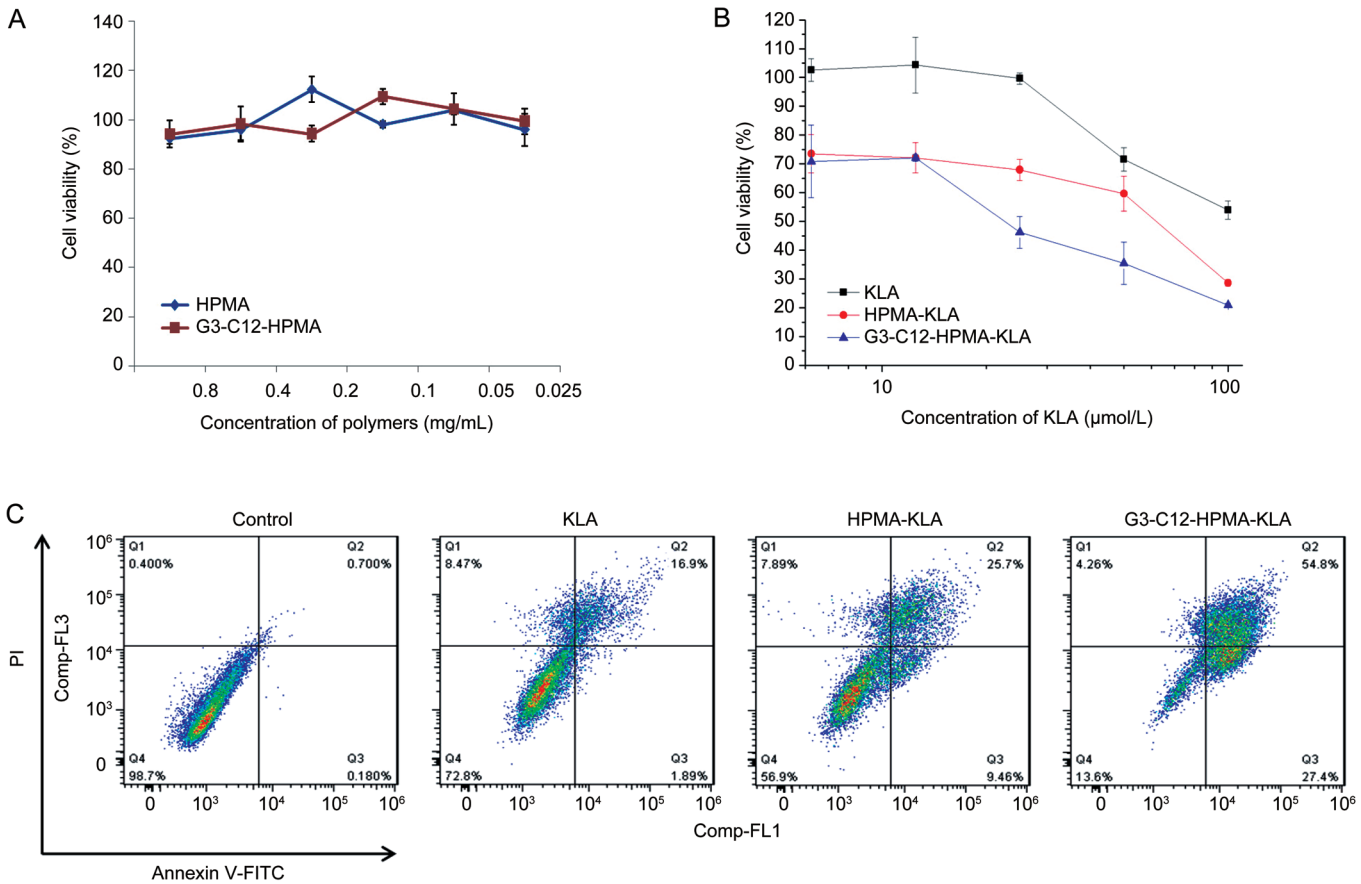


**Figure 7.** Cell cytotoxicity and proapoptosis effect of KLA peptide and KLA-loaded HPMA copolymers. (A) Biocompatibility investigation of drug-free carrier HPMA copolymer and G3-C12-HPMA copolymer. (B) Viability of PC-3 cells treated with predetermined concentration of free KLA, HPMA-KLA and G3-C12-HPMA-KLA, respectively. (C) Apoptosis assay of PC-3 cells after treatments as indicated for 24 h at the equivalent KLA concentration of 25 nmol/mL.

compatible *in vivo* as evidenced by the increased tumor accumulation and augmented tumor growth inhibition.

## Conclusion

In summary, we have demonstrated that a single G3-C12 ligand can sequentially target the PC-3 cell surface and intracellular mitochondria. G3-C12-HPMA-KLA was first internalized into PC-3 cells via the active recognition of galectin-3 overexpressed on the cell surface. After endocytosis, the KLA peptide triggered the re-distribution of galectin-3 to mitochondria. Thus, the specific binding between galectin-3 and the G3-C12 peptide directed G3-C12-HPMA-KLA to the mitochondria. Ultimately, the dual-targeting functionality of the G3-C12 peptide facilitated the KLA-mediated disruption of the mitochondrial membrane and resulted in improved therapeutic efficacy both *in vitro* and *in vivo*. The G3-C12 peptide may show some superiority over other targeting ligands with only one target site, as it can overcome both cellular and subcellular barriers and specifically travel with its receptor galectin-3 all the way from the cell surface to mitochondria. To the best of our knowledge, there has been no report on the sequential dual-targeting capability of the G3-C12 peptide thus far; we hope that our work could offer some interesting insights into the establishment of drug-delivery systems that can achieve subcellular-level targeting.

## Acknowledgements

The work was funded by the National Natural Science Foundation of China (81473167) and the Doctoral Fund of the Ministry of Education of China (2013018111001).

## Author contribution

Wei SUN, Zhi-rong ZHANG, and Yuan HUANG designed the research; Wei SUN, Lian LI, Li-jia LI, and Qing-qing YANG performed the research; Wei SUN and Lian LI analyzed the data; Wei SUN, Lian LI, and Yuan HUANG wrote the paper; Yuan HUANG revised the paper.

## References

1 Du J, Lane LA, Nie S. Stimuli-responsive nanoparticles for targeting the tumor microenvironment. J Control Release 2015; 219: 205–14.
2 Li L, Yang Q, Zhou Z, Zhong J, Huang Y. Doxorubicin-loaded, charge reversible, folate modified HPMA copolymer conjugates for active cancer cell targeting. Biomaterials 2014; 35: 5171–87.

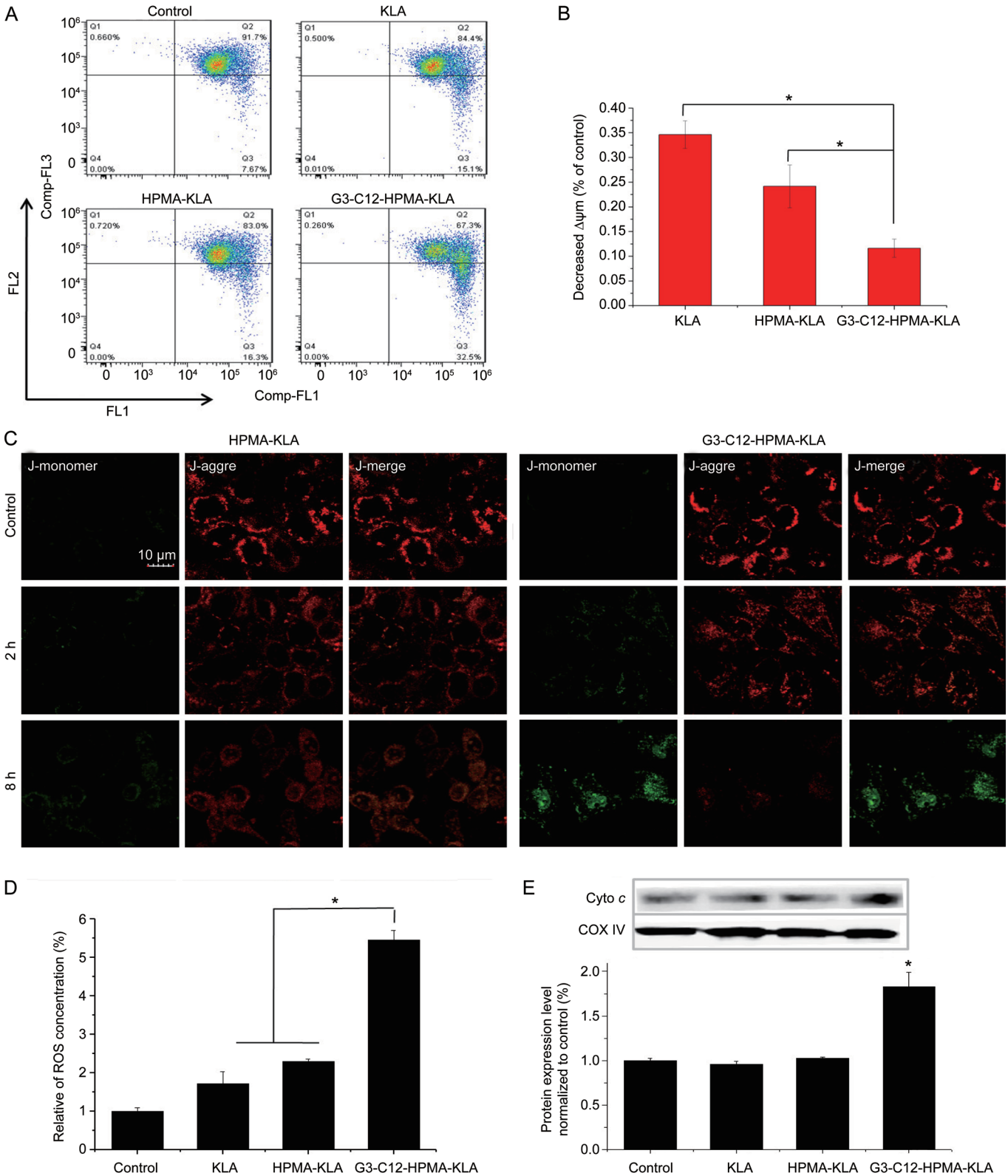


**Figure 8.** Mitochondria related apoptosis pathway. Relative fluorescent intensity of JC-1 aggregates and monomer (A) and change in mitochondrial membrane potential Δψm (B) of PC-3 cells treated with culture medium, KLA, HPMA-KLA, and G3-C12-HPMA-KLA for 24 h by flow cytometry. (C) CLSM images with JC-1 assay of PC-3 cells with HPMA-KLA and G3-C12-HPMA-KLA treatment for 0, 2, and 8 h, respectively. Scale bars represent 50 μm. (D) Changes of intracellular ROS generation induced by KLA, HPMA−KLA, and G3-C12-HPMA−KLA for 24 h. Cells incubated with 10 μmol/L DHE in PBS for 30 min and fluorescent intensity was measured by flow cytometry. (E) The protein expression level of cytochrome *c* was detected by Western blot after treatment with KLA, HPMA-KLA and G3-C12-HPMA-KLA for 24 h. COX IV was served as control. $^{*}P<0.05$ *vs* control.

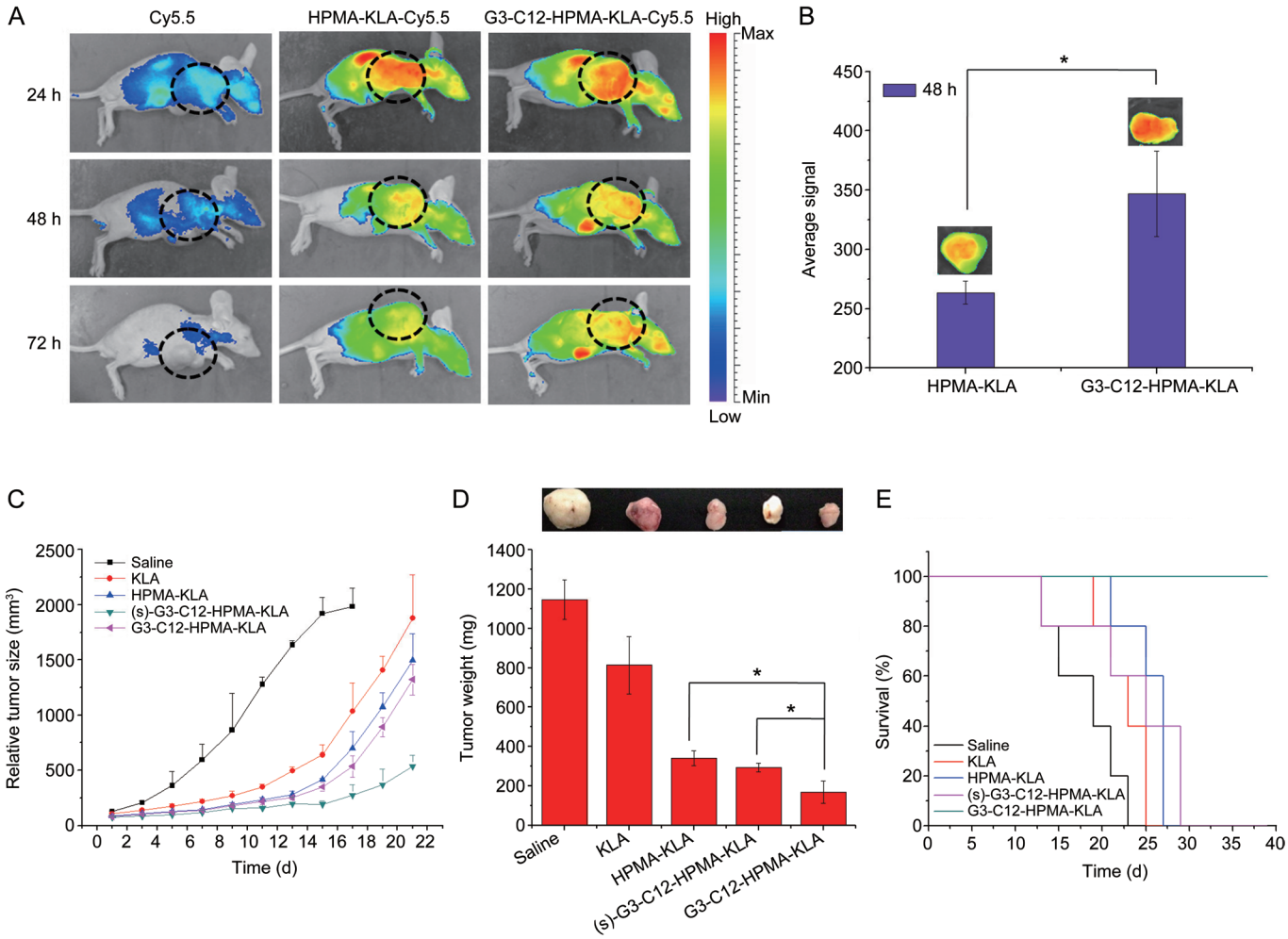


**Figure 9.** G3-C12 peptide enhances *in vivo* tumor accumulation and anticancer efficacy of KLA. (A) Real-time fluorescence imaging of PC-3 tumor-bearing mice after intravenous administration of Cy5.5, HPMA-KLA-Cy5.5 or G3-C12-HPMA-KLA-Cy5.5. (B) Quantization of fluorescence in tumors excised from PC-3 tumor-bearing mice two days after they received intravenous injection of HPMA-KLA-Cy5.5 and G3-C12-HPMA-KLA-Cy5.5. (C) Tumor growth, (D) tumor weight and (E) animal survival in a mouse model of PC-3 tumors following various treatments ($n$=6 per treatment).

3 Yang Y, Zhou Z, He S, Fan T, Jin Y, Zhu X, *et al.* Treatment of prostate carcinoma with (galectin-3)-targeted HPMA copolymer-(G3-C12)-5-fluorouracil conjugates. Biomaterials 2012; 33: 2260–71.
4 Li L, Sun W, Zhong J, Yang Q, Zhu X, Zhou Z, *et al.* Multistage nanovehicle delivery system based on stepwise size reduction and charge reversal for programmed nuclear targeting of systemically administered anticancer drugs. Adv Funct Mater 2015; 25: 4101–13.
5 Jiang L, Li L, He X, Yi Q, He B, Cao J, *et al.* Overcoming drug-resistant lung cancer by paclitaxel loaded dual-functional liposomes with mitochondria targeting and pH-response. Biomaterials 2015; 52: 126–39.
6 Mei L, Fu L, Shi K, Zhang Q, Liu Y, Tang J, *et al.* Increased tumor targeted delivery using a multistage liposome system functionalized with RGD, TAT and cleavable PEG. Int J Pharm 2014; 468: 26–38.
7 Kibria G, Hatakeyama H, Ohga N, Hida K, Harashima H. Dual-ligand modification of PEGylated liposomes shows better cell selectivity and efficient gene delivery. J Control Release 2011; 153: 141–8.
8 Kang B, Mackey MA, El-Sayed MA. Nuclear targeting of gold nanoparticles in cancer cells induces DNA damage, causing cytokinesis arrest and apoptosis. J Am Chem Soc 2010; 132: 1517–9.
9 Chen WH, Xu XD, Luo GF, Jia HZ, Lei Q, Cheng SX, *et al.* Dual-targeting pro-apoptotic peptide for programmed cancer cell death via specific mitochondria damage. Sci Rep 2013; 3: 3468.
10 Tijerina M, Kopeckova P, Kopecek J. Correlation of subcellular compartmentalization of HPMA copolymer-Mce(6) conjugates with chemotherapeutic activity in human ovarian carcinoma cells. Pharm Res 2003; 20: 728–37.
11 Jensen KD, Nori A, Tijerina M, Kopeckova P, Kopecek J. Cytoplasmic delivery and nuclear targeting of synthetic macromolecules. J Control Release 2003; 87: 89–105.
12 Callahan J, Kopecek J. Semitelechelic HPMA copolymers functionalized with triphenylphosphonium as drug carriers for membrane transduction and mitochondrial localization. Biomacromolecules 2006; 7: 2347–56.
13 Pan LM, Liu JN, He QJ, Shi JL. MSN-mediated sequential vascular-to-cell nuclear-targeted drug delivery for efficient tumor regression. Adv Mater 2014; 26: 6742–8.
14 Tang ZM, Li D, Sun HL, Guo X, Chen YP, Zhou SB. Quantitative control of active targeting of nanocarriers to tumor cells through optimization of folate ligand density. Biomaterials 2014; 35: 8015–27.

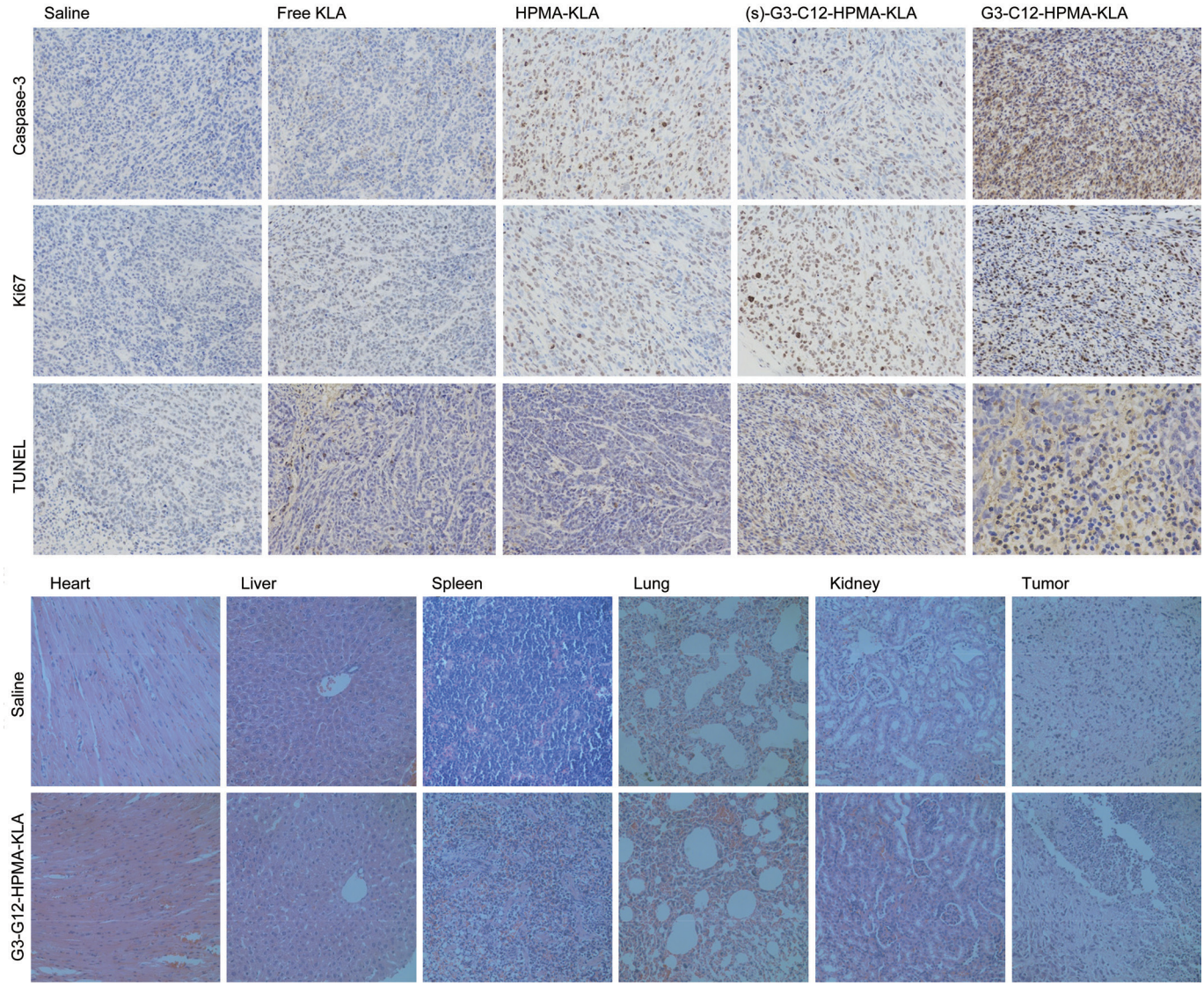


**Figure 10.** (A) Caspase-3, Ki67, and TUNEL staining of tumor tissues after treatment with various formulations. The Ki67-positive proliferating cells, caspase-3-positive and TUNEL-positive apoptotic cells were stained brown. (B) Histological evaluation of major organs (heart, liver, spleen, lung, kidney and tumor) from PC-3 xenograft model nude mice after treatment with saline (control) and G3-C12-HPMA-KLA. Tissues were stained with hematoxylin and eosin (200×).

15 Lee JH, Sahu A, Jang C, Tae G. The effect of ligand density on *in vivo* tumor targeting of nanographene oxide. J Control Release 2015; 209: 219–28.
16 Sun W, Li L, Yang Q, Shan W, Zhang Z, Huang Y. G3-C12 peptide reverses galectin-3 from foe to friend for active targeting cancer treatment. Mol Pharm 2015; 12: 4124–36.
17 Yang Y, Li L, Zhou Z, Yang Q, Liu C, Huang Y. Targeting prostate carcinoma by G3-C12 peptide conjugated N-(2-hydroxypropyl)methacrylamide copolymers. Mol Pharm 2014; 11: 3251–60.
18 Cieslewicz M, Tang J, Yu JL, Cao H, Zavaljevski M, Motoyama K, *et al.* Targeted delivery of proapoptotic peptides to tumor-associated macrophages improves survival. Proc Natl Acad Sci U S A 2013; 110: 15919–24.
19 Foillard S, Jin ZH, Garanger E, Boturyn D, Favrot MC, Coll JL, *et al.* Synthesis and biological characterisation of targeted pro-apoptotic peptide. Chembiochem 2008; 9: 2326–32.
20 Ellerby HM, Arap W, Ellerby LM, Kain R, Andrusiak R, Rio GD, *et al.* Anti-cancer activity of targeted pro-apoptotic peptides. Nat Med 1999; 5: 1032–8.
21 Javadpour MM, Juban MM, Lo WC, Bishop SM, Alberty JB, Cowell SM, *et al. De novo* antimicrobial peptides with low mammalian cell toxicity. J Med Chem 1996; 39: 3107–13.
22 Adar L, Shamay Y, Journo G, David A. Pro-apoptotic peptide-polymer conjugates to induce mitochondrial-dependent cell death. Polym Adv Technol 2011; 22: 199–208.
23 Chu DS, Bocek MJ, Shi J, Ta A, Ngambenjawong C, Rostomily RC, *et al.* Multivalent display of pendant pro-apoptotic peptides increases cytotoxic activity. J Control Release 2015; 20: 155–61.
24 Ulbrich K, Subr V, Strohalm J, Plocova D, Jelinkova M, Rihova B. Polymeric drugs based on conjugates of synthetic and natural macromolecules. I. Synthesis and physico-chemical characterisation. J Control Release 2000; 64: 63–79.

25 Rejmanová P, Labský J, Kopeček J. Aminolyses of monomeric and polymeric 4-nitrophenyl esters of N-methacryloylamino acids. Macromol Chem Phys 1977: 178: 2159–68.
26 Omelyanenko V, Kopeckova P, Gentry C, Kopecek J. Targetable HPMA copolymer-adriamycin conjugates. Recognition, internalization, and subcellular fate. J Control Release 1998; 53: 25–37.
27 Yang Q, Li L, Zhu X, Sun W, Zhou Z, Huang Y. The impact of the HPMA polymer structure on the targeting performance of the conjugated hydrophobic ligand. RSC Advances 2015; 5: 14858–70.
28 Yan J, Katz A. PectaSol-C modified citrus pectin induces apoptosis and inhibition of proliferation in human and mouse androgen-dependent and -independent prostate cancer cells. Integr Cancer Ther 2010; 9: 197–203.
29 Zhang Y, Li RJ, Ying X, Tian W, Yao HJ, Men Y, *et al.* Targeting therapy with mitosomal daunorubicin plus amlodipine has the potential to circumvent intrinsic resistant breast cancer. Mol Pharm 2011; 8: 162–75.
30 Ma X, Zhang LH, Wang LR, Xue X, Sun JH, Wu Y, *et al.* Single-walled carbon nanotubes alter cytochrome *c* electron transfer and modulate mitochondrial function. ACS Nano 2012; 6: 10486–96.
31 Rudolf E, Cervinka M. The role of intracellular zinc in chromium(VI)-induced oxidative stress, DNA damage and apoptosis. Chem Biol Interact 2006; 162: 212–27.
32 Yuan Y, Liu C, Qian J, Wang J, Zhang Y. Size-mediated cytotoxicity and apoptosis of hydroxyapatite nanoparticles in human hepatoma HepG2 cells. Biomaterials 2010; 31: 730–40.
33 Ahmed H, Cappello F, Rodolico V, Vasta GR. Evidence of heavy methylation in the galectin 3 promoter in early stages of prostate adenocarcinoma: development and validation of a methylated marker for early diagnosis of prostate cancer. Transl Oncol 2009; 2: 146–56.
34 Zou J, Glinsky VV, Landon LA, Matthews L, Deutscher SL. Peptides specific to the galectin-3 carbohydrate recognition domain inhibit metastasis-associated cancer cell adhesion. Carcinogenesis 2005; 26: 309–18.
35 Fukumori T, Oka N, Takenaka Y, Nangia-Makker P, Elsamman E, Kasai T, *et al.* Galectin-3 regulates mitochondrial stability and antiapoptotic function in response to anticancer drug in prostate cancer. Cancer Res 2006; 66: 3114–9.
36 Harazono Y, Kho DH, Balan V, Nakajima K, Zhang T, Hogan V, *et al.* Galectin-3 leads to attenuation of apoptosis through Bax heterodimerization in human thyroid carcinom a cells. Oncotarget 2014; 5: 9992–10001.
37 Inohara H, Raz A. Effects of natural complex carbohydrate (citrus pectin) on murine melanoma cell properties related to galectin-3 functions. Glycoconjuate J 1994; 11: 527–32.
38 Agemy L, Friedmann-Morvinski D, Kotamraju VR, Roth L, Sugahara KN, Girard OM, *et al.* Targeted nanoparticle enhanced proapoptotic peptide as potential therapy for glioblastoma. Proc Natl Acad Sci U S A 2011; 108: 17450–5.
39 Kroemer G, Galluzzi L, Brenner C. Mitochondrial membrane permeabilization in cell death. Physiol Rev 2007; 87: 99–163.
40 Chobot V, Hadacek F, Kubicova L. Effects of selected dietary secondary metabolites on reactive oxygen species production caused by iron(II) autoxidation. Molecules 2014; 19: 20023–33.
41 Susin SA, Lorenzo HK, Zamzami N, Marzo I, Snow BE, Brothers GM, *et al.* Molecular characterization of mitochondrial apoptosis-inducing factor. Nature 1999; 397: 441–6.
42 Kopecek J, Kopeckova P. HPMA copolymers: origins, early developments, present, and future. Adv Drug Delivery Rev 2010; 62: 122–49.
43 Li L, Sun W, Zhang Z, Huang Y. Time-staggered delivery of docetaxel and H1-S6A,F8A peptide for sequential dual-strike chemotherapy through tumor priming and nuclear targeting. J Control Release 2016; 232: 62–74.
44 Li N, Zhang CX, Wang XX, Zhang L, Ma X, Zhou J, *et al.* Development of targeting lonidamine liposomes that circumvent drug-resistant cancer by acting on mitochondrial signaling pathways. Biomaterials 2013; 34: 3366–80.
45 Chen S, Rong L, Lei Q, Cao PX, Qin SY, Zheng DW, *et al.* A surface charge-switchable and folate modified system for co-delivery of pro-apoptosis peptide and p53 plasmid in cancer therapy. Biomaterials 2016; 77: 149–63.
46 Yogev O, Pines O. Dual targeting of mitochondrial proteins: mechanism, regulation and function. Biochim Biophys Acta 2011; 1808: 1012–20.
47 Smith RA, Porteous CM, Gane AM, Murphy MP. Delivery of bioactive molecules to mitochondria *in vivo*. Proc Natl Acad Sci U S A 2003; 100: 5407–12.